An Efficient Uplink Multi-Connectivity Scheme for 5G Millimeter-Wave Control Plane Applications

Marco Giordani, *Student Member, IEEE*, Marco Mezzavilla, *Member, IEEE*, Sundeep Rangan, *Fellow, IEEE*, and Michele Zorzi, *Fellow, IEEE*

***Abstract*— The millimeter-wave (mm-wave) frequencies offer the potential of orders of magnitude that increases in capacity for next-generation cellular systems. However, links in mm-wave networks are susceptible to blockage and may suffer from rapid variations in quality. Connectivity to multiple cells at mm-wave and/or traditional frequencies is considered essential for robust communication. One of the challenges in supporting multi-connectivity in mm-waves is the requirement for the network to track the direction of each link in addition to its power and timing. To address this challenge, we implement a novel uplink measurement system that, with the joint help of a local coordinator operating in the legacy band, guarantees continuous monitoring of the channel propagation conditions and allows for the design of efficient control plane applications, including handover, beam tracking, and initial access. We show that an uplink-based multi-connectivity approach enables less consuming, better performing, faster and more stable cell selection, and scheduling decisions with respect to a traditional downlink-based standalone scheme. Moreover, we argue that the presented framework guarantees: 1) efficient tracking of the user in the presence of the channel dynamics expected at mm-waves and 2) fast reaction to situations in which the primary propagation path is blocked or not available.**

***Index Terms*— 5G, millimeter wave, multi-connectivity, initial access, handover, blockage, beam tracking.**

I. Introduction

THE millimeter wave (mm-wave) bands – roughly above 10 GHz – have attracted considerable attention for meeting the ever more demanding performance requirements of micro and picocellular networks [2]. These frequencies offer much more bandwidth than current cellular systems in the congested bands below 6 GHz, and initial capacity estimates have suggested that mm-wave networks can offer orders of magnitude higher bit-rates than 4G systems [3].

However, the increased carrier frequency of mm-wave systems makes the propagation conditions more demanding than at the lower frequencies traditionally used for wireless services, especially in terms of robustness. The communication quality between the user equipment (UE) and any one cell can indeed be highly variable as the movement of obstacles or even the changing position of the body relative to the mobile device can lead to rapid drops in signal strength. Moreover, mm-wave signals are blocked by many common building materials such as brick, and the human body can also significantly attenuate signals in the mm-wave range [4].

In this context, one likely key feature of cellular networks that can improve robustness is *multi-connectivity* (MC) [5]–[7], which enables each UE to maintain multiple possible signal paths to different cells so that drops in one link can be overcome by switching data paths. A multi-connectivity architecture can be both among multiple 5G mm-wave cells and between 5G mm-wave cells and traditional 4G cells below 6 GHz. Mobiles with such 4G/5G integration feature benefit from both the high bit-rates that can be provided by the mm-wave links and the more robust, but lower-rate, legacy channels, thereby opening up new ways to solve capacity issues, as well as new ways to provide good mobile network performance and robustness [8].

This paper addresses one of the key challenges in supporting multi-connectivity in heterogeneous networks (HetNets) with mm-wave cells, namely directional multi-cell channel tracking, measurement reporting and beam management. These operations are fundamental for cellular systems to properly perform a wide variety of control tasks including handover, path selection, and radio link failure (RLF) detection and recovery. However, while channel tracking and reporting is relatively straightforward in cellular systems at conventional frequencies, the mm-wave bands present several significant limitations, including: (i) the high variability of the channel in each link due to blockage [9]; (ii) the need to track multiple directions for each link [10]; and (iii) reports from the UE back to the cells must be made directional [11].

A. Contributions

The idea of using legacy connectivity for the management of the control plane is mainly motivated by the fact that 5G deployments would likely rely on the already deployed LTE core network (i.e., Evolved Packet Core (EPC)), thus initially avoiding a costly deployment of the new 5G infrastructures. Nevertheless, it is still unclear how multi-connectivity will be

Manuscript received July 21, 2017; revised April 27, 2018 and July 13, 2018; accepted July 22, 2018. Date of publication August 15, 2018; date of current version October 9, 2018. This paper was presented at the 15th Annual Mediterranean Ad Hoc Networking Workshop, Vilanova i la Geltru, Barcelona, Spain, June 2016 [1]. The associate editor coordinating the review of this paper and approving it for publication was G. Xue. *(Corresponding author: Marco Giordani.)*

M. Giordani and M. Zorzi are with the Department of Information Engineering, University of Padova, 35131 Padua, Italy (e-mail: giordani@dei.unipd.it; zorzi@dei.unipd.it).

M. Mezzavilla and S. Rangan are with NYU WIRELESS, Brooklyn, NY 11201 USA (e-mail: mezzavilla@nyu.edu; srangan@nyu.edu).

Color versions of one or more of the figures in this paper are available online at http://ieeexplore.ieee.org.

Digital Object Identifier 10.1109/TWC.2018.2864650

actually accomplished considering realistic 5G deployments. To address this challenge, in this paper we provide the first comprehensive numerical evaluation of the performance of a novel uplink (UL) multi-connectivity framework to enable fast, robust and efficient measurement reporting, beam management and cell selection operations.[1] In such a scheme, the UE directionally broadcasts sounding reference signals (SRSs) in time-varying directions that continuously sweep the angular space. Each potential serving cell scans all its angular directions and monitors the strength of the received SRSs. A centralized controller (that can be identified by an LTE eNB operating in the legacy band) obtains complete directional knowledge from all the potential cells in the network to make the optimal serving cell selection and scheduling decision. We note that the proposed scheme should not be confused with a mm-wave version of the Joint Transmission (JT) Coordinated MultiPoint (CoMP) nor the Coordinated Scheduling/Beamforming (CS/CB) CoMP [12], [13]. In the first case, multiple eNBs are simultaneously and cooperatively selected as transmission cells to achieve better reception of UEs at the cell edge. In the proposed method, although we measure control signals from multiple cells, the UE receives data from only one cell at a time. In the second case, UEs receive data only from their current serving cells, and eNBs share their associated users' channel state information and their relative scheduling information, with the overall goal of enabling inter-cell interference mitigation in a distributed way. In the proposed method, instead, coordination among different eNBs (possibly operating at different frequencies, e.g., in the legacy spectrum and at mm-waves) is exploited for the purpose of enabling fast and efficient handover, beam management and centralized control operations that would not be possible through traditional CoMP mechanisms. Importantly, unlike in standard CoMP, the UE does not need to maintain relative phase information for the links from different cells – a task that would be extremely difficult in a mm-wave setting due to the high Doppler. The proposed method is thus closer to carrier aggregation or fast handover.

As an extension of [1], in this paper we aim at comparing the performance of the proposed control framework that leverages multi-connectivity with that of a traditional downlink-based standalone (SA) scheme. We numerically show that:

- The implementation of a UL-based framework enables a faster and less energy consuming tracking of the channel quality over time at the mobile terminal. In fact, an uplink sounding scheme eliminates the need for the UE to send measurement reports back to the network and thereby removes a possible point of failure in the control signaling path. If digital beamforming (or beamforming with multiple analog streams) is available at the mm-wave cell, the directional scan time can be dramatically reduced when using UL-based measurements.
- The use of an MC approach enables a better resource allocation and mobility management compared to an SA configuration. In fact, LTE connectivity can offer a ready backup in case the mm-wave links suffer an outage and can be used to forward the scheduling and serving decisions to the user if the main propagation path is unavailable.
- The presented framework guarantees robust and stable communication quality in the presence of the channel variations and dynamics expected at mm-waves.

Furthermore, we give numerical evidence of how the proposed UL-based beam management framework enables the design of efficient 5G control plane applications and fundamental MAC layer functions that specify how a UE should connect to the network and preserve its connectivity. Specifically, our scheme allows for:

- Efficient and stable *handover*. Dense deployments of short range cells, as foreseen in future mm-wave cellular networks, may exacerbate frequent handovers between adjacent eNBs [14]. High throughput values can be continuously guaranteed when intensively monitoring the UE's channel quality over time (even when considering highly dynamic environments).
- Fast and fair *initial access*. Unlike in traditional attachment policies, by leveraging on the presence of the local coordinator, the initial association can be possibly performed by taking into account the instantaneous load conditions of the surrounding cells, thereby promoting fairness in the whole cellular network.
- Reactive *RLF detection and recovery*. In case the primary path is blocked, the UE is able to autonomously select a backup steering direction to recover connectivity without waiting for a handover to be eventually triggered.

Finally, we evaluate the performance of the presented framework by considering a detailed real-world measurement-based mm-wave channel scenario, for which we defined an innovative mobility model which accounts for the dynamics (in terms of both small and large scale fading) experienced by the mm-wave links. Most of the studies so far have been conducted in static conditions with minimal local blockage, whereas this is one of the first contributions in which a dynamic environment is considered.

B. Related Work

Channel estimation is relatively straightforward in LTE [15]. However, in addition to the rapid variations of the channel, transmissions at mm-waves are expected to be directional, and thus the network and the UE must constantly monitor the direction of transmission of each potential link. Tracking changing directions can slow the rate at which the network can adapt, and can be a major obstacle in providing robust service in the face of variable link quality. Moreover, the UE and its serving cell may only be able to listen to one direction at a time, thus making it hard to receive the control signaling necessary to switch paths.

The issue of designing efficient channel tracking solutions in highly mobile mm-wave scenarios has been recently addressed

[1]The performance of the proposed framework is assessed through system-level simulations. This approach has the benefit to include many more details than would be possible via analytical evaluations and allows to estimate the system performance accounting for realistic channel behaviors and detailed protocol implementations. Still, the definition of an accurate analytical model for dynamic scenarios remains a very relevant and timely topic for future research.

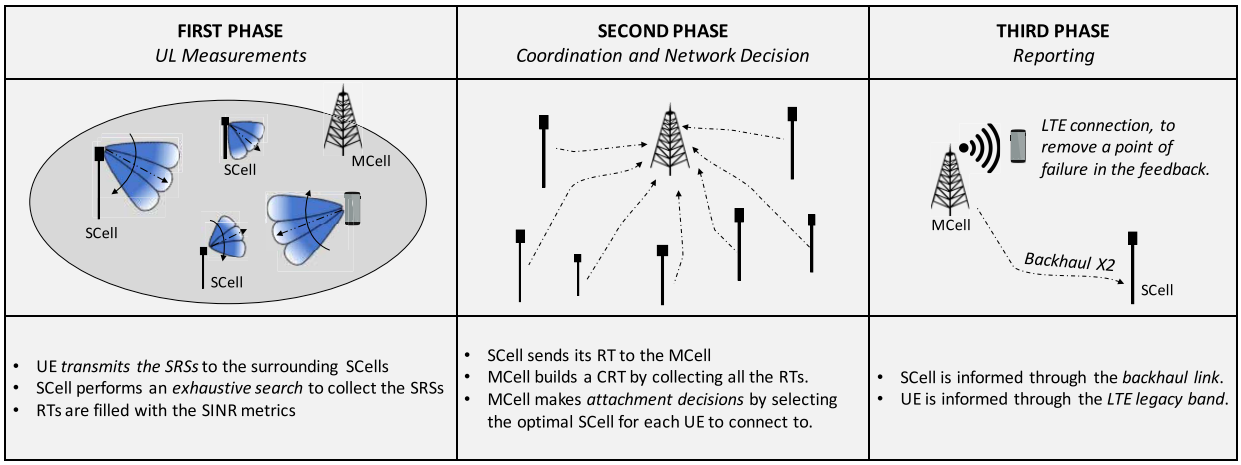

Fig. 1. Illustrative scheme of the MC procedure proposed in Sec. II.

in a number of literature works, e.g., in [16]. Other relevant papers on this topic include [17], in which a mobility-aware user association algorithm is proposed to overcome the limitations of the conventional power-based association approach typically implemented in legacy systems. Furthermore, in [18], the authors suggest making use of an extended Kalman filter to enable a static base station with digital beamforming capabilities to efficiently track a mobile node equipped with an analog beamformer. The proposed strategy delivers reduced alignment error and guarantees durable connectivity.

In these regards, dual-connectivity has been proposed in Release 12 of Long Term Evolution-Advanced (LTE-A) [19] to support inter-frequency and intra-frequency communication as well as connectivity to different types of base stations (e.g., macro and pico base stations) [20] and achieve more robust connectivity. However, these systems were designed for conventional frequencies, and did not address the directionality and variability of the channels present at mm-waves. Some other previous works, such as [21], consider the bands under 6 GHz as the only control channel for 5G networks, to provide robustness against blockage and wider coverage range. However, high capacities can also be obtained just exploiting the mm-wave frequencies. So, in [5], a multi-connectivity framework is proposed as a solution for mobility-related link failures and throughput degradation of cell-edge users, relying on the fact that the transmissions from cooperating cells are coordinated for both data and control signals. The work in [22] assumes a HetNet deployment of small cells and proposes that the control plane be handled centrally for small geographical areas whereas, for large geographical areas, distributed control should be used. However, the performance evaluation of small cells that use the same carrier frequency deployed over a relatively wider area has not yet been investigated. In [23], a novel approach for managing mobility through multi-connectivity in wireless networks is presented by leveraging device-to-device caching. The results show that the proposed solution provides handover failures minimization, reduced energy consumption, and seamless mobility in emerging dense heterogeneous networks.

Some other recent works (e.g., [24], [25]) illustrate how to exploit spatial congruence between signals in different frequency bands to extract channel parameters in mm-waves from side information obtained in another band. The results in [26] confirm that out-of-band information, although posing new challenges (most of which still remain unsolved) for practical 5G control plane management, can be exploited for mm-wave link establishment purposes.

Finally, in [27] we showed, through an extensive simulation campaign, that the proposed framework is suitable to enable fast network handover procedures. However, the present work is distinguished from [27] as we now investigate the performance of other interesting cellular control applications as well (i.e., initial access and RLF detection and recovery) while accounting for the dynamics that affect mm-wave propagation.

II. Uplink Multi-Connectivity Beam Management Framework

As previously discussed, in order to compensate for the increased path loss experienced at high frequency, UEs and mm-wave cells must establish highly directional transmissions to benefit from the resulting beamforming gain and sustain acceptable communication quality. Directional links, however, require fine and continuous alignment of the transmitter and receiver beams, achieved through a set of operations that the 3GPP has recently categorized under the term *beam management* [7]. In this section and as illustrated in Fig. 1, we propose an innovative framework to perform efficient beam management operations, whose performance will be investigated in Sec. V. Motivated by the fact that the increasing heterogeneity in cellular networks is making the role of the uplink much more important [28], we consider an *uplink* framework in which the measurements are based on reference signals transmitted by the mobile terminals rather than by the eNBs as in traditional cellular systems. Moreover, we consider a *multi-connectivity* framework in which eNBs operating at mm-waves use an LTE eNB as a support for the control plane management [7] and UEs maintain multiple possible

connections (i.e., LTE and mm-wave overlays) to different cells to provide connectivity in case of failure in one of the network interfaces.

We consider a scenario in which multiple UEs and mm-wave eNBs, which we refer to as SCells (Secondary Cells), are deployed under the coverage of one major node called MCell (Master Cell, in accordance with 3GPP LTE terminology), that here is typically an LTE eNB operating in the legacy band (although, functionally, the MCell can be any network entity that performs centralized handover and scheduling decisions). The SCells and the MCell are interconnected via traditional high-capacity backhaul X2 connections. In order to establish directional communications, the UEs and SCells select the most suitable direction of transmission from a predefined codebook of directions (each identified by a beamforming vector) that cover the whole angular space. We let N_{SCell} and N_{UE} be the number of directions at each SCell and UE, respectively.

The key challenge in implementing stable connectivity is that the network must continuously monitor the signal strength of all the direction pairs for each of the possible links and quickly adapt in case of disconnections. This is done by each SCell building a *report table* (RT) for each UE, based on the channel quality, i.e., the Signal-to-Interference-plus-Noise (SINR) ratio, of each receiving direction. This information is then used by the central entity to select the suitable beam or beams for both the SCells and the UEs to maintain the alignment. The system can be more precisely described as follows. Suppose that, in the considered area, M SCells and N UEs are deployed under the control of one MCell. The framework performs the beam management operations through three main phases, as explained below.

A. First Phase: UL Measurements

Each UE directionally broadcasts uplink sounding reference signals in dedicated slots, steering through directions d_u, $u \in \{1, \ldots, N_{\mathrm{UE}}\}$,[2] to cover the whole angular space. The SRSs are scrambled by locally unique identifiers (e.g., C-RNTI) that are known to the SCells. Each candidate serving SCell performs a directional beam sweep as well, scanning through directions D_ν, $\nu \in \{1, \ldots, N_{\mathrm{SCell}}\}$,[2] to monitor the strength of the received SRSs and capture the dynamics of the channel.[3] Based on the quality (i.e., measured in terms of SINR) of each receiving direction, the SCells fill their report tables as represented in Tab. I. Therefore, $\mathrm{RT}_{i,j}$ is an $N_{\mathrm{UE}} \times N_{\mathrm{SCell}}$ matrix in which each entry $\mathrm{SINR}_{i,j}(d_u, D_\nu)$ corresponds to the SINR that SCell_j, $j \in \{1, \ldots M\}$, receiving through direction D_ν, $\nu \in \{1, \ldots, N_{\mathrm{SCell}}\}$, measures from the SRS broadcast by UE_i, $i \in \{1, \ldots N\}$, transmitting through direction d_u, $u \in \{1, \ldots, N_{\mathrm{UE}}\}$. Given that each mm-wave SCell can potentially provide coverage for all N users in the MCell, each SCell will assemble N RTs, one for each active UE, as illustrated in Fig. 2.

[2]The directions are scanned one at a time if analog beamforming is used, or all at once if a digital architecture is adopted.

[3]The synchronization between the sweeping of the UEs and the listening of the SCells in the mm-wave band is guaranteed by assuming that the nodes have already exchanged some preliminary synchronization information through LTE.

TABLE I

AN EXAMPLE OF THE $\mathrm{RT}_{i,j}$ THAT SCELL_j, SCANNING THROUGH DIRECTIONS D_ν, $\nu \in \{1, \ldots, N_{\mathrm{SCell}}\}$, BUILDS BASED ON THE SRSs SENT FROM UE_i, TRANSMITTING THROUGH DIRECTIONS d_u, $u \in \{1, \ldots, N_{\mathrm{UE}}\}$

UE_i	SCell_j		
	D_1	$\ldots$	$D_{N_{\mathrm{SCell}}}$
d_1	$\mathrm{SINR}_{i,j}(d_1, D_1)$	$\ldots$	$\mathrm{SINR}_{i,j}(d_1, D_{N_{\mathrm{SCell}}})$
$\ldots$	$\ldots$	$\ldots$	$\ldots$
$d_{N_{\mathrm{UE}}}$	$\mathrm{SINR}_{i,j}(d_{N_{\mathrm{UE}}}, D_1)$	$\ldots$	$\mathrm{SINR}_{i,j}(d_{N_{\mathrm{UE}}}, D_{N_{\mathrm{SCell}}})$

TABLE II

AN EXAMPLE OF CRT, REFERRED TO N USERS AND M AVAILABLE mmWave SCELLS IN THE NETWORK. EACH PAIR IS THE MAXIMUM SHANNON RATE MEASURED IN THE BEST DIRECTION BETWEEN UE_i (d^*) AND SCELL_j (D^*), WITH THEIR BACKUP PAIR ($\widetilde{d}$, $\widetilde{D}$) CORRESPONDING TO THE SECOND BEST AVAILABLE BEAM

	SCell_1	$\ldots$	SCell_M
UE_1	$\mathrm{R}^*_{1,1}(d^*, D^*)$ *backup* $(\widetilde{d}, \widetilde{D})$	$\ldots$	$\mathrm{R}^*_{1,M}(d^*, D^*)$ *backup* $(\widetilde{d}, \widetilde{D})$
$\ldots$	$\ldots$	$\ldots$	$\ldots$
UE_N	$\mathrm{R}^*_{N,1}(d^*, D^*)$ *backup* $(\widetilde{d}, \widetilde{D})$	$\ldots$	$\mathrm{R}^*_{N,M}(d^*, D^*)$ *backup* $(\widetilde{d}, \widetilde{D})$

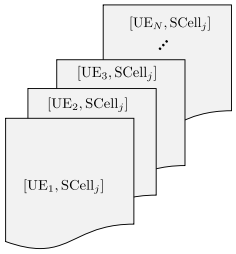

Fig. 2. Set of RTs assembled by SCell_j, based on the SRSs broadcast by all N UEs in the MCell.

B. Second Phase: Coordination and Network Decision

Once all the RTs have been filled, each mm-wave SCell sends this information, through the backhaul link, to the supervising MCell which, due to the knowledge gathered on the signal quality in each angular direction for each SCell-UE pair, is able to match the beams of the transceiver to provide maximum performance. To do so, unlike in legacy systems, the controller is aware of the instantaneous load of each mm-wave SCell, and beam selection can be made based on the maximum SINR (with some hysteresis) or on highest achievable Shannon rate.

In this last case, assume that N_j users are currently attached to SCell_j, and let W_{m} be the total available bandwidth at mm-waves. As illustrated in Tab. II, the MCell builds a *complete report table (CRT)*, i.e., an $N \times M$ matrix in which each entry $R_{i,j}(d^*, D^*)$ represents the highest Shannon rate between SCell_j, $j \in \{1, \ldots M\}$, and UE_i, $i \in \{1, \ldots N\}$, transmitting through directions D^* and d^*, respectively.

Formally:

$$R_{i,j}(d^*, D^*) = \underset{\substack{u=1,\ldots,N_{\mathrm{UE}} \\ \nu=1,\ldots,N_{\mathrm{SCell}}}}{\arg\max} \left\{ \frac{W_{\mathrm{m}}}{N_j} \log_2 \left[1 + \mathrm{SINR}_{i,j}(d_u, D\nu) \right] \right\}. \quad (1)$$

If a traditional max-SINR decision rule is considered instead, the CRT will incorporate information on the highest SINR experienced between SCell_j and UE_i, $\forall i, j$, transmitting through directions D^* and d^*, respectively, i.e.,

$$\mathrm{SINR}_{i,j}(d^*, D^*) = \underset{\substack{u=1,\ldots,N_{\mathrm{UE}} \\ \nu=1,\ldots,N_{\mathrm{SCell}}}}{\arg\max} \left\{ \mathrm{SINR}_{i,j}(d_u, D\nu) \right\}. \quad (2)$$

Notice that the CRT may also include information on the second[4] best direction pair $(\widetilde{d}, \widetilde{D})$ through which the highest Shannon rate (or SINR) was experienced. This knowledge can be used as a *backup* in case the primary propagation path is obstructed, as we will explain in Sec. III-C.

As soon as the CRT has been exhaustively filled, the MCell makes a network decision by selecting the best candidate mm-wave SCell for each UE to connect to. If the max-rate decision policy is selected, UE_i, $i \in \{1, \ldots N\}$, will attach to SCell_{j^*} such that

$$j^* = \underset{j=1,\ldots,M}{\arg\max} \left\{ R_{i,j}(d^*, D^*) \right\}. \quad (3)$$

This decision also embeds information on the optimal beam that the transceiver should select in order to establish aligned communications, i.e., d^* and D^*. Information on the backup directions for the UE and its serving SCell, i.e., $\widetilde{d}$ and $\widetilde{D}$ respectively, are provided as well.

C. Third Phase: Reporting

If the communication direction needs to be updated (i.e., beam tracking), the serving SCell needs to be switched (i.e., handover), or a secondary cell needs to be added or dropped, the MCell needs to inform both the UE and the designated mm-wave SCell. Since the UE may not be listening in the direction of the target SCell, the UE may not be able to hear a command from that cell. Moreover, since path switches and cell additions in the mm-wave regime are commonly due to link failures, the control link to the serving mm-wave cell may not be available either. To handle these circumstances, beam reporting leverages multi-connectivity, i.e., we propose that the path switch and scheduling commands be communicated over the coordinator operating in the legacy band. Therefore, for each UE in the network, the MCell notifies the corresponding optimal mm-wave SCell, via the high-capacity backhaul link, about the UE's desire to attach to it. It also embeds the best direction D^* that should be set to reach that user. Moreover, supposing that the UE has already set up a link to the LTE eNB on a legacy connection, the MCell sends to the UE, through an omnidirectional control signal at sub-6 GHz frequencies, the best user's direction d^* (together with its backup direction $\widetilde{d}$) to select to reach such candidate SCell. By this time, the best SCell-UE beam pair has been determined, therefore the transceiver can directionally communicate in the mm-wave band with the full beamforming gain.

[4]As specified by the 3GPP [29], the network nodes can potentially record information for a set of N_{best} available directions, where N_{best} can be configured to be 1 or more than 1. Such information can be used (i) as a backup in case the absolute best communication direction becomes unavailable, as suggested in the proposed beam management procedure, or (ii) to average the signal quality from the N_{best} best beams among all the available ones to perform a more robust attachment decision.

III. Enabling 5G Control Applications

As mentioned in Sec. I, existing control and mobility management procedures already implemented in a variety of traditional wireless systems should be revised and adapted to the unique mm-wave radio environment in which future networks are expected to operate.

Cellular: Next-generation cellular systems must provide a mechanism by which UEs and mm-wave eNBs establish highly directional transmission links – typically formed with high-dimensional phased arrays – to benefit from the resulting beamforming gain and balance for the increased isotropic pathloss experienced at high frequencies. In this context, directional links require precise alignment of the transmitter and receiver beams, an operation which might dramatically increase the time it takes to access the network, especially in the face of variable link quality [30]. Moreover, the dynamics of the mm-wave channel imply that the directional path to any cell can deteriorate rapidly, necessitating an intensive tracking of the UE.

Vehicular: Advanced and sophisticated sensors future cars will be equipped with will require an unprecedented amount of data to be exchanged, which goes beyond the capabilities of existing technologies and calls for innovative solutions [31]. On the one hand, the mm-wave band embeds certain desirable features for future vehicular communications and has the potential to support the expected bit-rate demands (in the order of terabytes per driving hour) of some advanced services [32]. On the other hand, there are still many concerns regarding its transmission characteristics in an automotive environment [33]. In highly dense or highly mobile vehicular scenarios, once the nodes are directionally connected, the corresponding peer may change frequently and may not last long enough to allow the completion of a data exchange, thus resulting in transmission errors and disconnections [34]. Moreover, the increased Doppler effect could make the assumption of channel reciprocity invalid and could impair the feedback over mm-wave links, which is a potential point of failure for beam sweeping. Periodic realignment of the beams is therefore required to maintain connectivity [35], [36].

802.11ad: The IEEE 802.11ad standard operates in the 60 GHz spectrum and therefore currently designed control protocols already address some of the challenges pertaining to a high-frequency environment [37]. However, most proposed solutions are unsuitable for the requirements of next-generation wireless systems, and present major limitations (e.g., they are appropriate for short-range, indoor scenarios, which do not match well the requirements of 5G systems). Therefore, new specifically designed solutions for dynamic networks need to be found.

As we will numerically show in Sec. V and discuss in Secs. III-A – III-C, we claim that faster, more efficient and more robust control plane applications (including handover, beam tracking, initial access, RLF recovery) can be enabled when considering a multi-connectivity architecture, compared to the case in which a standalone scheme is preferred.

A. Handover and Beam Tracking

Handover is performed when the UE moves from the coverage of one cell to the coverage of another cell and requests reassociation [38]. Beam tracking refers to the need for the UE to periodically adjust its steering direction to realign with its current serving eNB, as a consequence of network topology changes or channel adaptation. Frequent handover, even for fixed UEs, is a potential drawback of mm-wave systems due to their vulnerability to random obstacles, which is not the case in LTE. Dense deployments of short range eNBs, as foreseen in mm-wave networks, may exacerbate frequent handovers between adjacent eNBs. Loss of beamforming information due to channel change is another reason for handover and beam adaptation [14].

The literature on handover and beam tracking in traditional sub-6 GHz networks is quite mature, e.g., [15], [39], [40]. However, most works are specifically tailored to low-frequency legacy cellular systems, whose features are largely different from those of a mm-wave environment, preventing the proposed techniques from being applicable to next-generation 5G scenarios. On the other hand, papers on mobility management for mm-wave networks (e.g., [27], [41]–[44]) are very recent, since research in this field is just in its infancy.

As we will numerically show in Sec. V-C, we argue that the presented beam management framework leveraging multi-connectivity ensures efficient mobility management by (i) constantly monitoring the quality of the received signal at the SCell and at the UE through measurements in the mm-wave band, and (ii) exploiting the centralized MCell control over the network. Report tables make it possible to regularly determine (i) the UE's optimal mm-wave SCell to associate with (if handover is strictly required[5]), and (ii) the new directions d^* and D^* through which the UE in *connected mode* and its current serving SCell, respectively, should steer their beams to maintain alignment (if a simple beam adaptation operation is sufficient to avoid disconnections).

B. Initial Access

The procedure described in the previous subsection is referred to a UE that is already connected to the network. However, we claim that the uplink-based multi-connectivity framework proposed in Sec. II allows for fast initial access (IA) from *idle mode* too. Initial access [11] is the procedure by which a mobile terminal establishes an initial physical link connection with a cell, a necessary step to access the network. In LTE systems, IA is performed on omnidirectional channels [38], whereas directional beams are optionally formed only for data transmission. However, when operating at mm-waves, eNBs and UEs must determine suitable directions of transmission during IA as well, to overcome the increased isotropic pathloss experienced at higher frequencies.

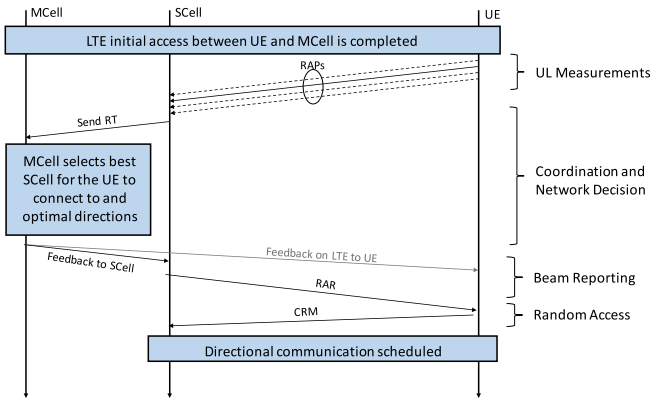

Fig. 3. Proposed initial access strategy based on the uplink multi-connectivity framework described in Sec. II.

Different initial access design options at mm-waves have been recently analyzed in [45]–[48] to evaluate coverage and access delay. In [11], [50], and [51], the authors have provided guidelines to characterize the optimal choice as a function of the system parameters. We refer to [11] for a more detailed survey of recent IA works. All of these methods are based on the current LTE design in which each cell broadcasts synchronization signals and each UE scans the directional space to find the optimal node to potentially connect to. A key result of these schemes is that the dominant delay in downlink-based IA arises in this initial sychronization phase.

Unlike in LTE schemes, we propose an IA strategy that is based on the channel quality of the UL rather than that of the DL signals. As illustrated in Fig. 3, the UE initially searches for synchronization signals from conventional LTE cells. This detection is fast since it can be performed omni-directionally and there is no need for directional scanning.[6] After that, the uplink reference signals (i.e., *random access preambles (RAPs)*, according to IA terminology), broadcast by the UEs, are collected by the SCells to build the report tables that will be used by the MCell to make the attachment decision and optimally match the beams of the transceiver. The decisions are forwarded (i) to the UEs via legacy omnidirectional messages, and (ii) to the SCells via backhaul links. As long as the best SCell-UE beam pair has been determined, *random access response (RAR)* signals and *connection request messages (CRMs)* are sent to exchange timing and power correction information and for contention resolution purposes, respectively [51].

[5]In order to reduce the handover frequency, more sophisticated decision criteria could be investigated, rather than triggering a handover every time a more suitable SCell is identified (i.e., the reassociation might be performed only if the SINR increases above a predefined threshold, with respect to the previous time instant). A more detailed discussion of the different handover paradigms is beyond the scope of this paper, and we refer the interested reader to [27] for further details.

[6]Under the assumption that the 5G mm-wave eNBs are roughly time synchronized to the 4G cell, and the round trip propagation times are not large, an uplink transmission from the UE will be roughly time aligned at any closeby mm-wave cell. For example, if the cell radius is 150 m (a typical mm-wave cell), the round trip delay is only 1 μs.

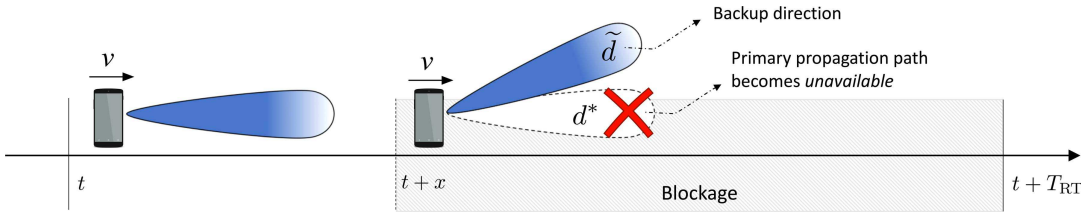

Fig. 4. RLF recovery procedure based on the uplink multi-connectivity framework described in Sec. II. At time t and $t+T_{\mathrm{RT}}$ the SCell collects an RT. At time $t+x$ a blockage event occurs and the UE, moving at constant velocity v, loses the connection with its current serving mm-wave SCell. The UE can promptly react to the channel failure by exploiting its backup direction $\widetilde{d}$.

The performance of the presented IA procedure will be evaluated in Sec. V-B.

C. Radio Link Failure Detection and Recovery

One of the key challenges that systems operating in the mm-wave bands have to cope with is the rapid channel dynamics. When the quality of an associated control channel falls below a certain threshold, i.e., in the case of RLF, mechanisms to recover acceptable communication capabilities (e.g., by adapting the node's steering direction or, as a last resort, by handing over to a stronger and more robust cell) need to be quickly triggered upon notifying the network [10]. Most literature on this topic refers to challenges that have been recently analyzed in the 60 GHz IEEE 802.11ad WLAN and WPAN scenarios, e.g., [26], [52]–[54].

In this context, we claim that the beam management framework proposed in Sec. II can be employed to partially overcome the link failure. We use Fig. 4 as a reference. Assume that, at time t, the UE, moving at constant speed v, is connected to SCell_{j^*}, $j^* \in \{1,\ldots,M\}$, through direction d^*. As soon as a blockage is detected, e.g., at time $t+x$, the UE may no longer be able to communicate since the optimal directional path connecting the endpoints is affected by the failure. If no actions are taken, the UE has to wait for a new instance of the CRT to be generated (at time $t+T_{\mathrm{RT}}$) before an alternative direction of transmission, able to circumvent the obstruction, is determined. One practical way to promptly react to the path impairment is by configuring the UE to communicate to SCell_{j^*} through its second best direction $\widetilde{d}$ as a sort of *backup solution* before the transceiver fully recovers the optimal beam configuration. Although $\widetilde{d}$ represents a suboptimal solution (since the optimal path is blocked), at least it allows the UE to experience a higher throughput than it would have achieved if no actions were taken.

The performance of the proposed RLF recovery solutions will be shown in Sec. V-D.

IV. Description of the Simulation Framework

In this section we present the system model we considered to evaluate the performance of the proposed control framework. The channel and mobility models are described in Secs. IV-A and IV-B, respectively, while the simulation parameters are illustrated in IV-C.

A. Channel Models

1) Millimeter-Wave Channel Model: The channel model we have implemented is based on recent real-world measurements at 28 GHz in New York City, and provides a realistic assessment of mm-wave micro and picocellular networks in a dense urban deployment. The parameters that are used to generate one instance of the channel matrix $\mathbf{H}$ include: (i) spatial clusters; (ii) fractions of power; (iii) angular beamspreads; and (iv) a small-scale fading model, massively affected by the Doppler shift, where each of the path clusters is synthesized with a large number of subpaths. A complete description of the channel parameters can be found in [3], [56], and [57].

The distance-based pathloss, which models Line-of-Sight (LoS), Non-Line-of-Sight (NLoS) and outage, is defined as $PL_{i,j}(r) = \alpha + \beta 10\log_{10}(r) + \xi_\sigma$, where r is the distance between the receiver j and the transmitter i and $\xi_\sigma \sim N(0,\sigma^2)$ represents the shadowing. For the NLoS case, $\alpha = 72.0$, $\beta = 2.92$ and $\sigma = 8.7$ dB while, for LoS, $\alpha = 61.4$, $\beta = 2$ and $\sigma = 5.8$ [3].

Due to the high pathloss experienced at mm-waves, multiple antenna elements with beamforming (BF) are essential to provide an acceptable communication range. The BF gain from SCell_j, receiving through direction D^*, to UE_i, transmitting through direction d^*, is given by

$$G_{\mathrm{BF}_{i,j}}(d^*, D^*) = \left| w^{\mathbb{R}x}_{\{D^*\}} \mathbf{H}_{i,j} w^{\mathbb{T}x}_{\{d^*\}} \right|^2 \tag{4}$$

where $\mathbf{H}_{i,j}$, with $i \in \{1,\ldots,N\}$ and $j \in \{1,\ldots,M\}$, is the channel matrix of the ij^{th} link, $w^{\mathbb{R}x}_{\{D^*\}} \in \mathbb{C}^{n_{\mathbb{R}x}}$ is the receive BF vector of the SCell and $w^{\mathbb{T}x}_{\{d^*\}} \in \mathbb{C}^{n_{\mathbb{T}x}}$ is the transmit BF vectors of the UE. Analog or digital BF architectures are typically considered. The former shapes the output beam with only one radio frequency (RF) chain, using phase shifters. This model saves power by using a single ADC but has limited flexibility since the SCells can only beamform in one direction at a time. A digital BF architecture, instead, provides the highest flexibility in shaping the beams, allowing transmission/reception in multiple directions simultaneously, but requires one RF chain per antenna element, thus potentially increasing the energy cost of the architecture [57].

The channel quality between SCell_j and UE_i is measured in terms of SINR, i.e.,

$$\mathrm{SINR}_{i,j}(d^*, D^*) = \frac{\frac{P_{\mathrm{TX_m}}}{PL_{i,j}(r)} G_{\mathrm{BF}_{i,j}}(d^*, D^*)}{\sum\limits_{k \neq j} \frac{P_{\mathrm{TX_m}}}{PL_{i,k}(r)} G_{\mathrm{BF}_{i,k}}(d^*, D^\dagger) + W_{\mathrm{m}} N_0}, \tag{5}$$

where $W_{\mathrm{m}} N_0$ is the thermal noise power. In (5), it is assumed that the UE is interfered by other SCells which point their beams towards random directions $D^\dagger$. However, to some extent, given the wide bandwidth, it is easy to orthogonalize

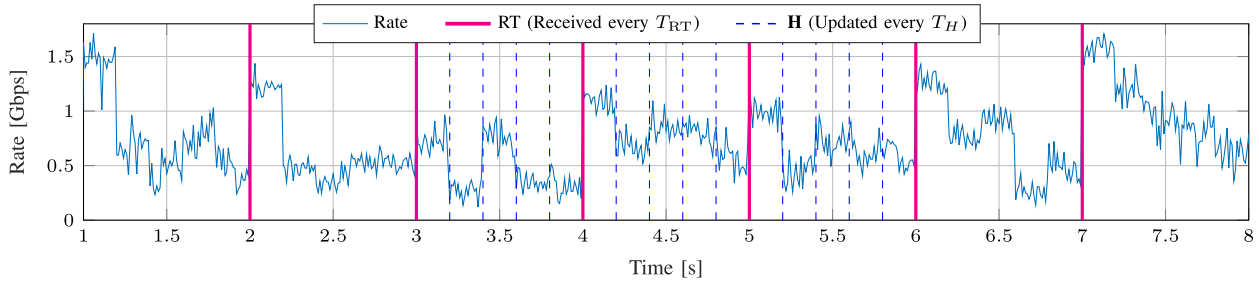

Fig. 5. Example of time-varying rate experienced by a user moving at speed $v = 20$ m/s in a scenario in which $M = 70$ SCell/km^2 are deployed. The RTs are generated every $T_{\mathrm{RT}} = 1$ s (vertical magenta lines), the small and large scale fading parameters of **H** vary every time slot, i.e., 1 ms, and every $T_H = 200$ ms (vertical blue dotted lines), respectively.

the SRSs across multiple users and we can assume that the SRS waveforms are transmitted over multiple sub-signals, each transmitted over a small bandwidth W_{sig}. The use of the sub-signals can provide frequency diversity, and narrowband signals in the control plane remove any inter-cell interference and support low power receivers with high SINR capabilities [45]. Finally, the rate R experienced by UE$_i$ connected to SCell$_j$ is approximated using the Shannon capacity:

$$R_{i,j}(d^*, D^*) = \frac{W_{\mathrm{m}}}{N_j} \log_2 \left[1 + \mathrm{SINR}_{i,j}(d^*, D^*)\right], \quad (6)$$

where N_j is the number of users that are currently being served by SCell$_j$ and W_{m} is the available total bandwidth.

2) LTE Channel: A connection to the LTE band is required when the mm-wave primary propagation path is obstructed or not available, or to reliably forward the scheduling/attachment decisions to the final user. According to the LTE 3GPP specifications in [19] and considering an outdoor dense scenario, a test UE at distance r (in km) from the LTE eNB is in LoS with probability

$$P_{\mathrm{LoS}}(r) = \min\left(\frac{0.018}{r}, 1\right)\left[1 - \exp\left(\frac{-r}{0.063}\right)\right] + \exp\left(\frac{-r}{0.063}\right) \quad (7)$$

and in NLoS with probability $P_{\mathrm{NLoS}}(r) = 1 - P_{\mathrm{NLoS}}(r)$. The pathloss is defined as

$$PL(r) = \begin{cases} 103.4 + 24.2 \log_{10}(r), & \text{w.p. } P_{\mathrm{LoS}}(r) \\ 131.1 + 42.8 \log_{10}(r), & \text{w.p. } P_{\mathrm{NLoS}}(r). \end{cases} \quad (8)$$

When considering an LTE connection, signals are assumed to be exchanged through omnidirectional channels. Therefore, if we deploy just one LTE eNB in the reference scenario, the quality of the received information is measured, in terms of SNR, by:

$$\mathrm{SNR} = \frac{P_{\mathrm{TX_L}}/PL(r)}{W_{\mathrm{L}} N_0}, \quad (9)$$

where $W_{\mathrm{L}} N_0$ is the thermal noise power. The rate can be computed according to Eq. (6).

B. Mobility Model

One of the key challenges for cellular systems in the mm-wave bands is the rapid channel dynamics, e.g., the Doppler shift whose effect increases with speed. In order to simulate such dynamics, we propose a mobility model in which the small and the large scale fading parameters of the mm-wave **H** matrix are periodically updated, to emulate short variations and sudden changes of the perceived channel, respectively.

The Doppler shift and the spatial signatures are updated at every time slot, according to the user speed and its position, in terms of angle of arrival (AoA) and departure (AoD). The distance-based pathloss is also updated, but we maintain the same pathloss state (LoS, NLoS or outage) recorded in the previous complete update of the **H** matrix. On the other hand, to capture the effects of the long term fading, the **H** matrix parameters (i.e., the number of spatial clusters and subpaths, the fractions of power, the angular beamspreads and the pathloss conditions) are completely updated every T_H s, for all the mm-wave links between each UE and each SCell. We recall that this may cause the user to switch from a certain pathloss state to another (e.g., from LoS to NLoS, to simulate the presence of an obstacle between transmitter and receiver), with a consequent sudden drop of the channel quality by many dBs.

The beamforming vectors are not adapted when the **H** matrix is updated. We need to wait for a new RT to be collected, i.e., every T_{RT}, to detect the (possibly changed) channel propagation conditions and properly react, i.e., by adapting the directions through which the UE and the designated SCell steer their beams. Frequent RTs (small T_{RT}) and slowly varying channels (large T_H) result in a good monitoring of the user and good average channel gains. In Sec. V-C we show how the values of T_{RT} and T_H affect the communication quality.

As an example, in Fig. 5 we plot the rate experienced by a test user, moving at speed $v = 20$ m/s along a straight line during a random simulation. The large scale fading parameters of **H** are updated every $T_H = 200$ ms, while the beam configuration is updated every $T_{RT} = 1$ s. We see that, at time $t = 2^-$ s, the rate has strongly degraded, since the UE has moved without updating its beam steering direction and thus has misaligned from its serving SCell. However, at time

TABLE III
MAIN SIMULATION PARAMETERS

Parameter	Value	Description
W_{m}	1 GHz	Bandwidth of mmWave SCells
$f_{\mathrm{c,m}}$	28 GHz	mmWave carrier frequency
$P_{\mathrm{TX,m}}$	30 dBm	Transmission power of mmWave SCells
W_{L}	20 MHz	Bandwidth of LTE eNB
$f_{\mathrm{c,L}}$	2 GHz	LTE carrier frequency
$P_{\mathrm{TX,L}}$	46 dBm	Transmission power of LTE eNB
Γ_{out}	-5 dB	Minimum SINR threshold
$N_{\mathrm{ANT,SCell}}$	8×8	SCell UPA MIMO array size
$N_{\mathrm{ANT,UE}}$	4×4	UE UPA MIMO array size
N_{SCell}	16	SCell scanning directions
N_{UE}	8	UE scanning directions
N_m	10	UEs per mmWave SCell
v	20 m/s	UE speed
T_{per}	200 μs	SRS inter-transmission time
T_{sig}	10 μs	SRS duration
ϕ_{ov}	5%	Overhead

$t = 2$ s, a new CRT has been generated and the transceiver is finally able to update its beam configuration (by performing a beam switch operation) or the UE can hand over (by choosing a serving SCell providing better communication performance), thus recovering the maximum achievable rate. We notice that wide rate collapses (e.g., at time $t = 3.2$ s or $t = 5.2$ s) mainly refer to pathloss state changes (i.e., from LoS to NLoS), caused by the update of the large scale fading parameters of $\mathbf{H}$, while the rapid fluctuations of the rate are due to the adaptation of the small scale fading parameters of the channel (and mainly to the Doppler effect experienced by the moving UE).

C. Simulation Scenario

The parameters used to run our simulations are based on realistic system design considerations and are summarized in Tab. III. Our results are derived through a Monte Carlo approach, where multiple independent simulations of duration T_{sim} are repeated, to get different statistical quantities of interest. In each experiment: (i) under the control of a single MCell operating in the legacy band, we deploy M mm-wave SCells and N UEs, according to a Poisson Point Process (PPP) and as done in [58], with an average density of $N_m = 10$ users per cell (as foreseen in [59] for a dense urban environment); (ii) we run the beam management framework described in Sec. II by establishing a mm-wave link between each SCell-UE pair and collecting the SINR values at each SCell, according to Eq. (5), when the transceiver performs the sequential scan; and (iii) we select the most profitable mm-wave SCell the user should attach to, according to either a maximum SINR or a maximum Shannon rate policy. The load of each SCell is determined according to the procedure described in [60]. If a maximum Shannon rate policy is chosen, the UEs are initially associated with the SCell offering the highest signal strength, then we iteratively pick one UE at a time updating the SCell it is connected to according to Eq. (3). This iterative procedure is repeated by re-allocating a random UE at each step, until convergence is reached. Border effects are avoided by considering a sufficiently large simulation area and evaluating the performance of a test UE in the center of the scenario. At the end of the procedure, N_j mobile terminals will be associated with SCell_j, $\forall j \in \{1, \ldots, M\}$.

We consider an SINR threshold $\Gamma_{\mathrm{out}} = -5$ dB, assuming that, if $\mathrm{SINR}_{i,j}(d^*, D^*) < \Gamma_{\mathrm{out}}$, no control signals are collected when UE_i transmits through direction d^* and SCell_j receives through direction D^*. Decreasing Γ_{out} would allow finding more SCells, at the cost of designing more complex (and expensive) receiving schemes, able to detect the intended signal in more noisy channels. If a multi-connectivity approach is chosen, the UE may still be able to reach the MCell (by establishing a connection over the LTE band) when the signal quality is below Γ_{out}.

The antenna elements are arranged as uniform planar arrays (UPAs) at both the mm-wave SCells and the UE, since they can synthesize a 3D beam and offer easy packageability on handsets (e.g., at 28 GHz, a 4×4 UPA array has a size of roughly 1.5 cm $\times$ 1.5 cm [45]). SCells are equipped with 8×8 arrays, which allow them to steer beams in $N_{\mathrm{SCell}} = 16$ directions; the user exploits an array of 4×4 antennas, steering beams through $N_{\mathrm{UE}} = 8$ angular directions.[7]

In the first phase of the proposed control framework, we alternate portions of time in which SRSs are transmitted in brief intervals of length T_{sig}, and intervals of length $T_{\mathrm{per}} \gg T_{\mathrm{sig}}$ in which each SCell and each UE handle their usual traffic operations. We took $T_{\mathrm{sig}} = 10\ \mu s$, which is sufficiently small to ensure that the channel will be coherent even at the very high frequencies for mm-waves, and $T_{\mathrm{per}} = 200\ \mu s$, in order to maintain a constant overhead of $\phi_{\mathrm{ov}} = 5\%$.[8]

V. RESULTS AND PERFORMANCE EVALUATION

In this section, we present some simulation results to:

(i) compare the performance of the multi-connectivity framework proposed in Sec. II with a mm-wave-only standalone scheme in terms of delay, throughput, energy consumption and stability;
(ii) give numerical evidence of the performance of several control applications (i.e., handover, beam tracking, initial access, RLF recovery) which can be enabled in next-generation mm-wave systems by the presented measurement reporting framework;
(iii) demonstrate how the variability of the mm-wave channel affects the performance of a cellular network (mainly in terms of achievable throughput).

A. Comparison With Downlink Standalone Scheme

In this section, we focus on the differences between a non-standalone deployment exploiting multi-connectivity and a standalone architecture, according to whether the control plane is managed with the support of an LTE overlay or not, respectively. While in a non-standalone deployment the network

[7] In this work, we assume a 2D structure for the cells. Nevertheless, our system is easily customizable and allows for the design of an advanced 3D scanning technique as well. However, such a choice would lead to an increase of the time required to complete each iteration of the presented measurement reporting scheme, without providing any further noticeable insights.

[8] The values of T_{per} and T_{sig} have been chosen according to the analysis in [11], [46], and [50] and are based on simulations that enable reliable detection with an overhead of $\phi_{\mathrm{ov}} = 5\%$. However, the proposed framework is general and its parameters can be tuned according to the peculiarities of any specific simulation environment.

TABLE IV

DELAY D TO COMPLETE EACH ITERATION OF EITHER THE UPLINK MULTI-CONNECTIVITY MEASUREMENT FRAMEWORK DESCRIBED IN SEC. II OR A TRADITIONAL DOWNLINK STANDALONE APPROACH. A COMPARISON AMONG DIFFERENT BF ARCHITECTURES (ANALOG AND FULLY DIGITAL) IS PERFORMED. WE ASSUME $T_{\mathrm{sig}} = 10\ \mu$s, $T_{\mathrm{per}} = 200\ \mu$s (TO MAINTAIN AN OVERHEAD $\phi_{\mathrm{ov}} = 5\%$), $N_{\mathrm{SCell}} = 16$ AND $N_{\mathrm{UE}} = 8$. DIGITAL BEAMFORMING IS APPLIED AT THE RECEIVER

BF	**UL Scheme** UEs transmit SCells receive	**DL Scheme** UEs receive SCells transmit
Analog	$N_{\mathrm{SCell}}N_{\mathrm{UE}}T_{\mathrm{per}}$ (25.6 ms)	$N_{\mathrm{SCell}}N_{\mathrm{UE}}T_{\mathrm{per}}$ (25.6 ms)
Digital	$\frac{N_{\mathrm{SCell}}N_{\mathrm{UE}}T_{\mathrm{per}}}{N_{\mathrm{SCell}}}$ (1.6 ms)	$\frac{N_{\mathrm{SCell}}N_{\mathrm{UE}}T_{\mathrm{per}}}{N_{\mathrm{UE}}}$ (3.2 ms)

elements can maintain multiple possible connections in the mm-wave and the LTE bands, with the standalone option there is no LTE control plane, therefore the integration between LTE and the mm-wave cells is not supported.

1) Delay: We define as D the time *delay* required to complete each iteration of either the uplink multi-connectivity framework presented in this work or a traditional downlink standalone scheme. We claim that the first phase of the proposed framework (i.e., UL measurements) dominates the overall delay performance, provided that (i) the time for beam switching is in the scale of nanoseconds, and so it can be neglected [61]; (ii) in the second phase of the procedure, RTs are sent through the X2 links, which may be wired or wireless backhaul and whose latency is assumed to be negligible [27]; and (iii) in the third phase of the procedure, the network decisions are forwarded to the UEs through omnidirectional LTE messages, whose latency is ignored if the UEs have already set up a link to the MCell.

According to Sec. IV-C, the scanning for the SRSs in each SCell-UE direction will require $N_{\mathrm{SCell}}N_{\mathrm{UE}}/L$ scans, where L is the number of directions in which the receiver can look at any one time. Since there is one scanning opportunity every T_{per}, the total delay is

$$D = \frac{N_{\mathrm{SCell}}N_{\mathrm{UE}}T_{\mathrm{per}}}{L}. \tag{10}$$

The value of L depends on the BF capabilities (and the array size). In the UL-based design, $L = 1$ if the SCell receiver has analog BF and $L = N_{\mathrm{SCell}}$ if it has a fully digital transceiver. Similarly, in the DL, $L = 1$ if the UE receiver has analog BF and $L = N_{\mathrm{UE}}$ if it has a fully digital transceiver. Tab. IV compares the resulting delays for UL- and DL-based designs depending on the BF capabilities of the receiver. We see that the UL design offers a significantly reduced access delay when a digital architecture is preferred and makes it possible to complete every repetition of the measurement reporting framework every at least 1.6 ms (when considering an overhead $\phi_{\mathrm{ov}} = 5\%$). The main reason is that we usually consider $N_{\mathrm{SCell}} \gg N_{\mathrm{UE}}$, due to the base station's less demanding space constraints with respect to a mobile terminal: a larger number of antenna elements can be packed at the SCell side, with a consequently higher number of directions that can potentially be scanned simultaneously through a digital BF scheme.

TABLE V

RATE $\mathbb{E}[R]$ EXPERIENCED WHEN EITHER THE MULTI-CONNECTIVITY FRAMEWORK DESCRIBED IN SEC. II OR A STANDALONE APPROACH IS USED. $T_H = 100$ ms, $T_{RT} = 300$ ms

M [SCell/km^2]	**Multi-connectivity**	**Standalone**
4	8.19 Mbps	5.5 Mbps
10	41.09 Mbps	35.4 Mbps
20	122.9 Mbps	121 Mbps
40	360.42 Mbps	357.6 Mbps
70	778.87 Mbps	777.4 Mbps
90	1103.6 Mbps	1103.6 Mbps

2) Throughput: In Tab. V, we evaluate the average rate $\mathbb{E}[R]$ experienced by the UE when either a multi-connectivity or a traditional standalone framework is applied, for different values of the SCell density M. In general, $\mathbb{E}[R]$ increases with M since the inter-cell distance is reduced and each UE finds a closer SCell (showing better channel propagation conditions) to associate with.

Moreover, we observe that the rate achievable with the first solution is higher than with the second one. The reason is that, when relying on the LTE eNB for dealing with outage events, the UE experiences a non-zero throughput, in contrast to the standalone configuration which cannot properly react to a situation where no mm-wave SCells are within reach. Although the gap between the two architectures is quite remarkable when considering very sparse environments, i.e., $M < 20$ SCell/km^2 (in those scenarios, most UEs experience outage, making the fallback to the LTE eNB a vital option for sustainable connectivity), the design of MC solutions may be desirable for several other reasons ranging from reduced energy consumption to increased robustness, and reactive link failure recovery, as summarized in Sec. V-E.

Finally, rate gains will likely be even more significant for increasing values of T_{RT}. In fact, less frequent tracking operations might lead to a more remarkable channel degradation between the transmitter and the receiver, making the fallback to LTE an increasingly attractive option to restore an adequate communication quality.

3) Energy Consumption: The energy consumption (E_C) can be evaluated as the product between the power (P_C) and the time delay (D) required to complete each iteration of each approach.[9] According to Tab. IV, when considering an uplink multi-connectivity scheme, digital BF is used at the SCell side while analog BF is preferred at the UE side, and $D^{\mathrm{MC}} = 1.6$ ms. Therefore:

$$E^{\mathrm{MC}}_{C,\mathrm{SCell}} = P^{\mathrm{DBF}}_{C} \cdot D^{\mathrm{MC}} \quad E^{\mathrm{MC}}_{C,\mathrm{UE}} = P^{\mathrm{ABF}}_{C} \cdot D^{\mathrm{MC}} \tag{11}$$

For a downlink standalone configuration, analog BF is used at the SCell side while digital BF is preferred at the UE side,

[9]The total power consumption (P_C) of each beamforming scheme is evaluated according to [63] and [64], in which $b = 3$ quantization bits are used by the Analog-to-Digital Converter block.

TABLE VI

ENERGY E_C TO COMPLETE EACH ITERATION OF EITHER THE UPLINK MULTI-CONNECTIVITY MEASUREMENT FRAMEWORK DESCRIBED IN SEC. II OR A TRADITIONAL DOWNLINK STANDALONE APPROACH. A DIGITAL BF CONFIGURATION IS APPLIED AT THE RECEIVER SIDE. $T_{\text{per}} = 200\ \mu$s, $N_{\text{SCell}} = 16$ AND $N_{\text{UE}} = 8$

Network Entity	**UL Scheme** UEs transmit SCells receive	**DL Scheme** UEs receive SCells transmit
SCell	1.7477 J	0.0665 J
UE	0.0287 J	0.8739 J

and $D^{\text{SA}} = 3.2$ ms. Therefore

$$E^{\text{SA}}_{C,\text{SCell}} = P^{\text{ABF}}_{C} \cdot D^{\text{SA}} \quad E^{\text{SA}}_{C,\text{UE}} = P^{\text{DBF}}_{C} \cdot D^{\text{SA}} \tag{12}$$

In Tab. VI, we compare the energy performance of the two approaches. It is evident that, although the UL scheme is more consuming at the SCell side, it is more energy efficient at the UE side. This represents a very relevant feature of the proposed multi-connectivity framework since mobile terminals are the most *energy-constrained* network entities, due to their limited battery capacity (contrary to the infrastructure nodes which are typically connected to the power grid and therefore do not suffer from strict energy requirements). We therefore claim that a UL framework, able to reduce the energy consumption of the mobile terminal by around 30 times with respect to its DL counterpart (with the settings of Tab. VI), should be preferred to enable a more efficient mobility management scheme.

4) Robustness: In order to compare the robustness of the multi-connectivity and the standalone configurations, following the analysis we proposed in [27], we use the ratio

$$\rho_{\text{var}} = \frac{\text{STD}(R)}{\mathbb{E}[R]}, \tag{13}$$

where $\mathbb{E}[R]$ is the mean value of the throughput measured for each approach and $\text{SRD}(R)$ is its standard deviation. High values of ρ_{var} reflect remarkable channel instability, thus the rate would be affected by local variations and periodic degradations.

Let $\rho^{\text{MC}}_{\text{var}}$ and $\rho^{\text{SA}}_{\text{var}}$ be the variance ratios of Eq. (13) for the multi-connectivity and the standalone configurations, respectively. From Fig. 6, we observe that $\rho^{\text{MC}}_{\text{var}}$ is lower than $\rho^{\text{SA}}_{\text{var}}$, for each value of the density M, making it clear that the LTE eNB employed in a MC configuration can stabilize the rate, which is not subject to significant variations. In fact, in the portion of time in which the UE would experience zero gain if a standalone architecture were implemented, the rate would suffer a noticeable discrepancy with respect to the LoS values, thus increasing the rate variance throughout the simulation. This is not the case for the MC configuration, in which the UE can always be supported by the LTE eNB, even when a blockage event affects the scenario. This result is fundamental for real-time applications, which require a long-term stable throughput to support high data rates and a consistently acceptable Quality of Experience for the users.

Finally, we observe that, in general, the stability of the network rate increases with M (showing smaller values of ρ_{var}),

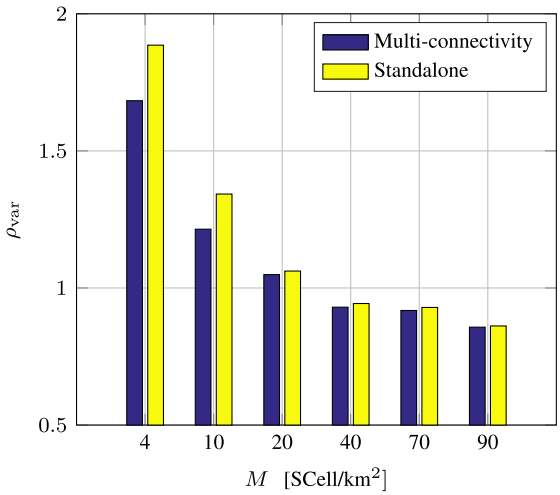

Fig. 6. Average ratio ρ_{var} vs. SCell density, showing the stability of the channel during the simulation.

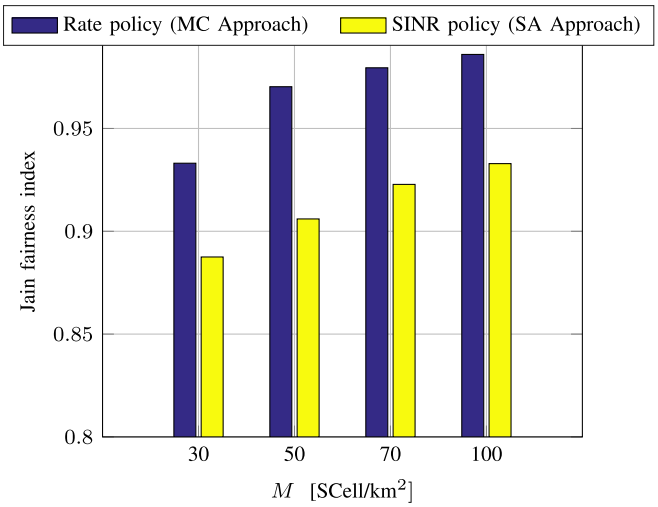

Fig. 7. Jain's fairness index of the rate vs. SCell density, for the initial access procedure. UEs within an area of radius equal to 70 m attach to their best SCell according to a maximum rate or maximum SINR policy.

due to the more consistent values of SINR (and rate) that are guaranteed in this case. Furthermore, in denser environments and as the probability of pathloss outage decreases, the gap between the two configurations decreases, as the role of the LTE eNB becomes less relevant.

B. Initial Access Performance

As assessed in Sec. V-A, for initial access, in addition to the time required for directional sweeping, there is also a delay related to the beam reporting operations, which differs according to the architecture being used. When considering a standalone configuration, the UE may not be able to receive from the optimal mm-wave link if not properly aligned, so beam reporting may require an additional sweep at the UE side, thereby further increasing the time it takes to access the network. If an MC architecture is preferred, instead, the beam decision is forwarded through the LTE interface, which makes the beam reporting reactiveness equal to the latency of a legacy

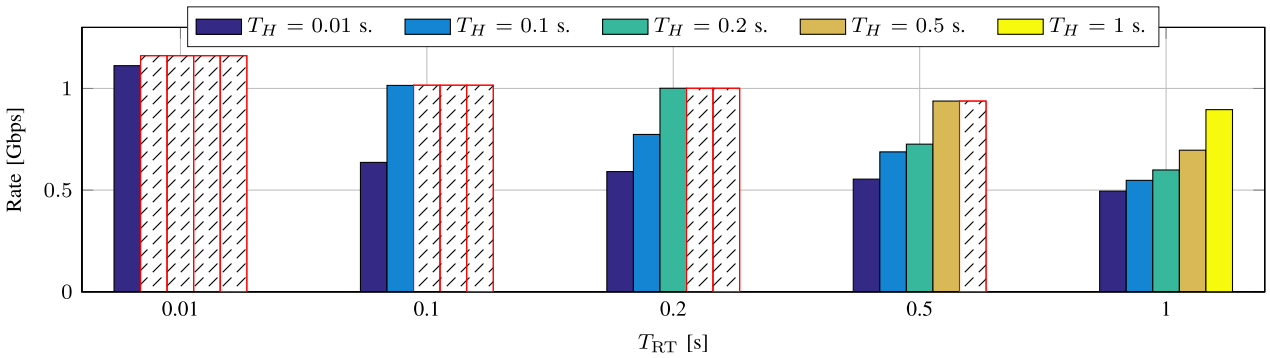

Fig. 8. Average rate vs. RT periodicity T_{RT}, for different values of T_H. The mm-wave SCell density is kept constant at $M = 70$ SCell/km^2. Striped bars are referred to uninteresting cases, since $T_{\mathrm{RT}} < T_H$. The user's speed is $v = 20$ m/s.

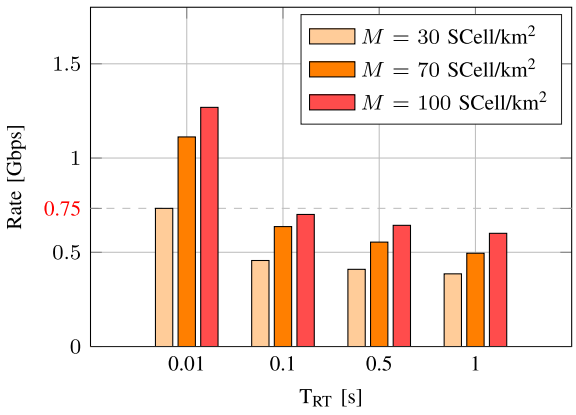

(a) Average rate vs. RT periodicity T_{RT}. The large scale fading parameters of **H** are updated every $T_H = 10$ ms.

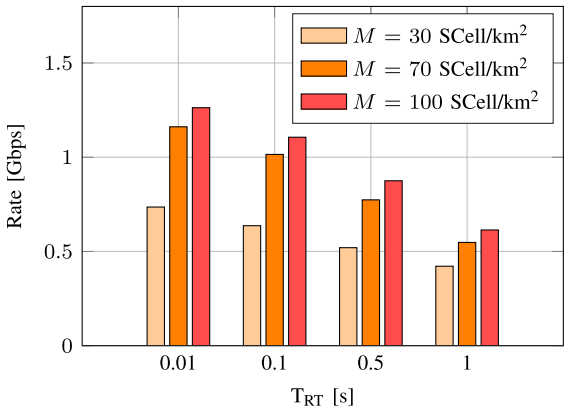

(b) Average rate vs. RT periodicity T_{RT}. The large scale fading parameters of **H** are updated every $T_H = 100$ ms.

Fig. 9. Results of the handover and beam tracking simulations, for different SCell densities. The user's speed is $v = 20$ m/s.

LTE connection. Faster attachment decisions can therefore be guaranteed when MC is chosen.

We also claim that the use of the supervising LTE MCell enables a fairer cell selection as well. Unlike in the traditional procedures in which the users are not aware of the current state of the surrounding cells, the UE may connect to the SCell providing either the maximum SINR (max-SINR rule) or the maximum Shannon rate (max-rate rule), depending on what is considered more convenient, thereby introducing new ways of providing fair and robust network association. In order to compare the two presented attachment policies, we use *Jain's fairness index*, which is used to determine whether UEs are receiving a fair share of the system resources and are thus experiencing a rate comparable to that of other UEs in the system. This index is defined as [64]:

$$J = \frac{\left(\sum_{i=1}^{N} R_i\right)^2}{N \sum_{i=1}^{N} R_i^2}, \tag{14}$$

where N is the number of users in the system and R_i is the rate experienced by the i-th user. The result ranges from $1/N$ (worst case – most unfair) to 1 (best case – most fair), and is maximum when all users receive the same allocation.

In Fig. 7, we plot Jain's fairness index for the rate experienced by users within an area of radius equal to 70 m, when attaching according to either a max-rate rule (by exploiting the MC procedure) or a max-SINR rule (as in traditional schemes). As expected, in the first case higher fairness is provided to the network: asymptotically, users accessing the network will likely find all the SCells in the same load conditions, guaranteeing comparable rates. On the other hand, in the second case, UEs will tend to connect to the same SCells showing the instantaneous highest signal strengths (and thus overloading them), and avoiding instead nodes that provide lower SINR values (but possibly higher rates, due to their low traffic loads).

We finally notice that Jain's fairness index in Fig. 7 increases with M for both schemes. In fact, when densifying the network, the SCells ensure more similar propagation conditions to the users, which in turn experience more balanced SINR (and rate) values.

C. Handover Performance

The test user moves at a constant speed $v = 20$ m/s towards a specific direction. Due to its mobility and to the variability of the mm-wave channel over time, it needs to periodically hand over or switch its transmitting beam, to recover a good communication quality. The large scale fading parameters of the channel are updated every T_H, while the small scale fading parameters are constantly updated every time slot. Every T_{RT},

the MCell can select, by looking at the best saved entry, the new serving SCell for the UE, or just select the new beam pair the transceiver has to set in order to maximize the communication throughput. We just consider the case $T_{\mathrm{RT}} \geq T_H$, as otherwise the rate would almost be constant for all values of T_H (since the beam pair would be updated before the channel even changes its large scale fading parameters).

According to Fig. 8, when T_{RT} increases, the average rate decreases, since fewer RTs are exchanged and the beam pair between the user and its serving SCell is monitored less frequently. This means that, when the channel changes (due to a pathloss condition modification or to a variation of the propagation characteristics) or when the user misaligns with its SCell (due to its motion), the communication quality is not immediately recovered and the throughput is affected by portions of time where suboptimal network settings are chosen. We also observe that, when T_H increases, the average rate also increases since the channel varies less rapidly, so the rate can assume more stable values even if the SCell-UE beam pair is monitored less frequently. In fact, even if a change in the **H** matrix's large scale fading parameters represents the strongest cause for the user's rate slump, if we consider slowly varying and stable channels, we can accept fewer report tables (and consequently trigger fewer handover and beam switch operations) and still provide a sufficiently good communication quality.

As already mentioned, Fig. 9 demonstrates that the average rate increases with M. Moreover, higher rates are experienced when $T_H = 100$ ms (Fig. 9(b)), with respect to the 10 ms case, since the channel changes less rapidly. Additionally, Fig. 9(a) exemplifies how a 0.75 Gbps rate can be achieved either with a 30 SCell/km^2 density and 10 ms T_{RT}, or with a 100 SCell/km^2 density and 100 ms T_{RT}: the tradeoff varies between infrastructure cost and signaling overhead.

Finally, it is interesting to notice that the main advantage when increasing the cell density is observed from $M = 30$ SCell/km^2 to $M = 70$ SCell/km^2. In fact such rate gain reflects the transition from a user outage regime to a LoS/NLoS regime while, as we persistently keep on densifying the network, the deployment of more SCells leads to a considerable increase of the system complexity, while providing a limited increase of the rate.

D. RLF Recovery Performance

According to the scenario described in Sec. III-C, we define $R^{(d^*)}$ as the optimal rate experienced when no obstacles affect the signal propagation (the UE will communicate through its optimal direction d^*), and $R^{(\widetilde{d})}$ as the suboptimal rate experienced when the backup beam pair $\widetilde{d}$ is selected, as the primary path is not available.

Assume that a blockage event is detected at time $T_{\mathrm{arr}} \sim \mathcal{U}(0, T_{\mathrm{RT}})$, and lasts for T_B s. We aim at finding the *rate gain* (R_G), namely the ratio between the rate experienced when the MC procedure is employed to establish a backup beam pair between the UE and its serving SCell after a blockage is detected (R_{WB}), and the rate perceived when no actions are taken (R_{OB}). We focus on the situation in which the obstacle is no longer present when the new CRT is generated ($T_{\mathrm{RT}} \geq 2T_B$), otherwise the beam pair would be updated when the obstacle is still obstructing the best path, thus still reducing the average rate. Then, the rate R_{WB} experienced when reacting after the blockage is detected by selecting the backup direction $\widetilde{d}$ to communicate can be computed (for a fixed time window T_{RT}), as:

$$R_{\mathrm{WB}} = \frac{R^{(d^*)}T_{\mathrm{arr}} + R^{(\widetilde{d})}T_B + R^{d^*}(T_{\mathrm{RT}} - T_{\mathrm{arr}} - T_B)}{T_{\mathrm{RT}}} = \frac{R^{(d^*)}(T_{\mathrm{RT}} - T_B) + R^{(\widetilde{d})}T_B}{T_{\mathrm{RT}}} \tag{15}$$

If no actions are taken, after the obstacle has been detected, the rate R_{OB} is:

$$R_{\mathrm{OB}} = \frac{R^{(d^*)}T_{\mathrm{arr}} + 0T_B + R^{(d^*)}(T_{\mathrm{RT}} - T_{\mathrm{arr}} - T_B)}{T_{\mathrm{RT}}} = \frac{R^{(d^*)}(T_{\mathrm{RT}} - T_B)}{T_{\mathrm{RT}}} \tag{16}$$

The average rate gain (R_G) between the two options is finally defined as:

$$R_G = \frac{R_{\mathrm{WB}}}{R_{\mathrm{OB}}} - 1 = \frac{R^{(\widetilde{d})}}{R^{(d^*)}} \cdot \frac{T_B}{T_{\mathrm{RT}} - T_B} \tag{17}$$

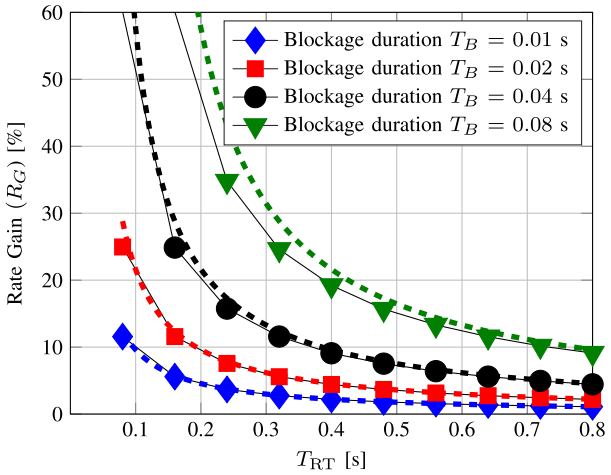

Fig. 10. Rate gain experienced when applying a backup procedure for the RLF recovery vs. RT periodicity T_{RT}, for different blockage scenarios. The obstacle duration is T_B and is detected after T_{arr}.

In Fig. 10, we first notice that $R_G > 0$ for all values of T_{RT} and T_B, making it clear that having a second available link (in case the primary one is blocked) guarantees improved communication throughput performance with respect to a traditional scheme in which a backup configuration is not available, as expected. Furthermore, when T_{RT} is sufficiently large, e.g., when $T_{RT} \gg 2T_B$, the simulation curves asymptotically overlap with the dashed lines plotting Eq. (17). Fig. 10 shows also that, for a fixed blockage duration T_B, as T_{RT} increases, the rate gain R_G decreases. In fact the portion of time in which the user would experience zero throughput (if no actions are taken when the primary path is obstructed) proportionally decreases within the time window of length

T_{RT}, making it less convenient to select a backup beam pair to overcome the blockage issue.

Finally, we see that, when T_B increases, the rate gain R_G increases as well, due to the increased enhancement provided by the use of a suboptimal beam pair after a blockage event occurs, with respect to the baseline algorithm in which no actions are taken till the reception of a new CRT.

E. Final Comments

To sum up, a comparison between the uplink multi-connectivity framework proposed in this work and a traditional downlink standalone approach has been made. Specifically, we concluded that a DL configuration, although being in line with the 3GPP design for next-generation wireless systems, is characterized by increased energy consumption at the UE side and less reactive mobility management operations with respect to a UL scheme.

Moreover, we showed that mobiles implementing MC can benefit from both the high bit-rates provided by the mm-wave links and the more robust, but lower-capacity, legacy channels. Conversely, with the standalone option, there is no LTE control plane and the integration between LTE and mm-waves is not supported. We concluded that MC

(i) offers significantly reduced access delays when a digital beamforming architecture is chosen;
(ii) leveraging on the LTE eNB to deal with outage events, guarantees higher average data rates to the system, especially when considering sparse environments;
(iii) enables an energy-efficient mobility management scheme for the mobile terminal, the most energy-constrained entity in the cellular network;
(iv) reduces the variations which usually affect the mm-wave channel, thus stabilizing the rate and improving the performance of real-time applications requiring long-term stable throughput;
(v) enables a centralized beam decision and, unlike in traditional attachment policies based on signal quality measurements, makes user associations taking into account the instantaneous load conditions of the surrounding cells, thereby promoting fairness in the network.

Although the aforementioned benefits were proven particularly significant in sparsely deployed networks (e.g., rural environment, highway scenarios), we showed that the proposed framework still enables efficient 5G control plane applications even in more dense networks. More specifically, we demonstrated that MC enables

(i) prompt handover and beam tracking operations even for highly dynamic scenario;
(ii) fast and fair initial access operations, if a max-rate attachment policy is chosen (while also reducing the impact of the overhead in the beam reporting phase);
(iii) an efficient radio link failure recovery, for UEs in connected mode, when a backup steering direction is set in case the primary path is obstructed.

VI. Conclusions and Future Work

A challenge for the feasibility of a 5G mm-wave system is the high susceptibility to the rapid channel dynamics that affect a mm-wave environment. In order to deal with these channel variations, a periodic directional sweep should be performed, to constantly monitor the directions of transmission of each potential link and to adapt the beam steering when a power signal drop is detected. In this work, we have presented a measurement reporting system that allows a supervising centralized entity, such as a base station operating in the legacy band, to periodically collect multiple reports on the overall channel propagation conditions, to enable efficient scheduling and mobility management decisions. We argue that, unlike traditional downlink standalone schemes, the proposed uplink strategy that leverages multi-connectivity enables more rapid, robust, and energy efficient network operations for UEs in connected and idle modes, in particular when considering very unstable channels and highly populated systems.

As part of our future work, we will design control applications that monitor and keep memory of the received signal strength variance, to better capture the dynamics of the channel and steer the cell selection strategy of delay-sensitive applications towards more robust cells.

References

[1] M. Giordani, M. Mezzavilla, S. Rangan, and M. Zorzi, "Multi-connectivity in 5G mmWave cellular networks," in *Proc. 15th Annu. Medit. Ad Hoc Netw. Workshop (Med-Hoc-Net)*, Vilanova i la Geltrú, Spain, Jun. 2016, pp. 1–7.
[2] S. Rangan, T. S. Rappaport, and E. Erkip, "Millimeter-wave cellular wireless networks: Potentials and challenges," *Proc. IEEE*, vol. 102, no. 3, pp. 366–385, Mar. 2014.
[3] M. R. Akdeniz *et al.*, "Millimeter wave channel modeling and cellular capacity evaluation," *IEEE J. Sel. Areas Commun.*, vol. 32, no. 6, pp. 1164–1179, Jun. 2014.
[4] J. Lu, D. Steinbach, P. Cabrol, and P. Pietraski, "Modeling the impact of human blockers in millimeter wave radio links," *ZTE Commun. Mag.*, vol. 10, no. 4, pp. 23–28, 2012.
[5] F. B. Tesema, A. Awada, I. Viering, M. Simsek, and G. P. Fettweis, "Mobility modeling and performance evaluation of multi-connectivity in 5G intra-frequency networks," in *Proc. IEEE Globecom Workshops (GC Wkshps)*, Dec. 2015, pp. 1–6.
[6] *Evolved Universal Terrestrial Radio Access (E-UTRA) and NR; Multi-Connectivity*, document TS 37.340 (Release 15), 3GPP, 2018.
[7] *Study on New Radio Access Technology: Radio Access Architecture and Interfaces*, document TR 38.801, 3GPP, 2017.
[8] *Microwave Towards 2020*, Ericsson, Stockholm, Sweden, Sep. 2015.
[9] K. Haneda *et al.*, "Indoor 5G 3GPP-like channel models for office and shopping mall environments," in *Proc. IEEE Int. Conf. Commun. Workshops (ICCW)*, May 2016, pp. 694–699.
[10] M. Giordani, M. Mezzavilla, A. Dhananjay, S. Rangan, and M. Zorzi, "Channel dynamics and SNR tracking in millimeter wave cellular systems," in *Proc. Eur. Wireless (EW)*, Oulu, Finland, May 2016, pp. 306–313.
[11] M. Giordani, M. Mezzavilla, and M. Zorzi, "Initial access in 5G mmWave cellular networks," *IEEE Commun. Mag.*, vol. 54, no. 11, pp. 40–47, Nov. 2016.
[12] R. Irmer *et al.*, "Coordinated multipoint: Concepts, performance, and field trial results," *IEEE Commun. Mag.*, vol. 49, no. 2, pp. 102–111, Feb. 2011.
[13] H. Sun, W. Fang, J. Liu, and Y. Meng, "Performance evaluation of CS/CB for coordinated multipoint transmission in LTE-A downlink," in *Proc. IEEE 23rd Int. Symp. Pers. Indoor Mobile Radio Commun. (PIMRC)*, Sep. 2012, pp. 1061–1065.
[14] H. Shokri-Ghadikolaei *et al.*, "Millimeter wave cellular networks: A MAC layer perspective," *IEEE Trans. Commun.*, vol. 63, no. 10, pp. 3437–3458, Oct. 2015.
[15] S. Schwarz, C. Mehlführer, and M. Rupp, "Calculation of the spatial preprocessing and link adaption feedback for 3GPP UMTS/LTE," in *Proc. IEEE Conf. Wireless Adv. (WiAD)*, Jun. 2010, pp. 1–6.

[16] J. Palacios, D. De Donno, and J. Widmer, "Tracking mm-Wave channel dynamics: Fast beam training strategies under mobility," in *Proc. IEEE Conf. Comput. Commun. (INFOCOM)*, Apr. 2017, pp. 1–9.

[17] A. S. Cacciapuoti, "Mobility-aware user association for 5G mmWave networks," *IEEE Access*, vol. 5, pp. 21497–21507, 2017.

[18] S. Jayaprakasam, X. Ma, J. W. Choi, and S. Kim, "Robust beam-tracking for mmWave mobile communications," *IEEE Commun. Lett.*, vol. 21, no. 12, pp. 2654–2657, Dec. 2017.

[19] *Technical Specification Group Radio Access Network; Study on Small Cell Enhancement for (E-UTRA) and (e-TRAN); Higher Layer Aspects (Release 12)*, document TR 36.842, 3GPP, 2013.

[20] A. Zakrzewska, D. López-Pérez, S. Kucera, and H. Claussen, "Dual connectivity in LTE HetNets with split control- and user-plane," in *Proc. IEEE Globecom Workshops (GC Wkshps)*, Dec. 2013, pp. 391–396.

[21] Z. He, S. Mao, and T. S. Rappaport, "Minimum time length link scheduling under blockage and interference in 60 GHz networks," in *Proc. IEEE Wireless Commun. Netw. Conf. (WCNC)*, Mar. 2015, pp. 837–842.

[22] V. Yazıcı, U. C. Kozat, and M. O. Sunay, "A new control plane for 5G network architecture with a case study on unified handoff, mobility, and routing management," *IEEE Commun. Mag.*, vol. 52, no. 11, pp. 76–85, Nov. 2014.

[23] O. Semiari, W. Saad, M. Bennis, and B. Maham, "Caching meets millimeter wave communications for enhanced mobility management in 5G networks," *IEEE Trans. Wireless Commun.*, vol. 17, no. 2, pp. 779–793, Feb. 2018.

[24] N. Gonzalez-Prelcic, A. Ali, V. Va, and R. W. Heath, Jr., "Millimeter-wave communication with out-of-band information," *IEEE Commun. Mag.*, vol. 55, no. 12, pp. 140–146, Dec. 2017.

[25] A. Ali and R. W. Heath, Jr., "Compressed beam-selection in millimeterwave systems with out-of-band partial support information," in *Proc. IEEE Int. Conf. Acoust., Speech Signal Process. (ICASSP)*, Mar. 2017, pp. 3499–3503.

[26] T. Nitsche, A. B. Flores, E. W. Knightly, and J. Widmer, "Steering with eyes closed: mm-Wave beam steering without in-band measurement," in *Proc. IEEE Conf. Comput. Commun. (INFOCOM)*, Apr./May 2015, pp. 2416–2424.

[27] M. Polese, M. Giordani, M. Mezzavilla, S. Rangan, and M. Zorzi, "Improved handover through dual connectivity in 5G mmWave mobile networks," *IEEE J. Sel. Areas Commun.*, vol. 35, no. 9, pp. 2069–2084, Sep. 2017.

[28] J. Oueis and E. C. Strinati, "Uplink traffic in future mobile networks: Pulling the alarm," in *Proc. Int. Conf. Cogn. Radio Oriented Wireless Netw.* Grenoble, France: Springer, 2016, pp. 583–593.

[29] *Measurement Configuration for CSI-RS*, document TDOC R2-1704103, 3GPP, Ericsson, 2017.

[30] F. Boccardi, R. W. Heath, Jr., A. Lozano, T. L. Marzetta, and P. Popovski, "Five disruptive technology directions for 5G," *IEEE Commun. Mag.*, vol. 52, no. 2, pp. 74–80, Feb. 2014.

[31] S. A. A. Shah, E. Ahmed, M. Imran, and S. Zeadally, "5G for vehicular communications," *IEEE Commun. Mag.*, vol. 56, no. 1, pp. 111–117, Jan. 2018.

[32] V. Va, T. Shimizu, G. Bansal, and R. W. Heath, Jr., "Millimeter wave vehicular communications: A survey," *Found. Trends Netw.*, vol. 10, no. 1, pp. 1–113, 2016.

[33] M. Giordani, A. Zanella, and M. Zorzi, "Millimeter wave communication in vehicular networks: Challenges and opportunities," in *Proc. 6th Int. Conf. Mod. Circuits Syst. Technol. (MOCAST)*, May 2017, pp. 1–6.

[34] M. Giordani, M. Rebato, A. Zanella, and M. Zorzi, "Coverage and connectivity analysis of millimeter wave vehicular networks," *Ad Hoc Netw.*, to be published. [Online]. Available: https://arxiv.org/abs/1803.01136

[35] J. Choi, V. Va, N. Gonzalez-Prelcic, R. Daniels, C. R. Bhat, and R. W. Heath, Jr., "Millimeter-wave vehicular communication to support massive automotive sensing," *IEEE Commun. Mag.*, vol. 54, no. 12, pp. 160–167, Dec. 2016.

[36] V. Va, T. Shimizu, G. Bansal, and R. W. Heath, Jr., "Beam design for beam switching based millimeter wave vehicle-to-infrastructure communications," in *Proc. IEEE Int. Conf. Commun. (ICC)*, May 2016, pp. 1–6.

[37] T. Nitsche, C. Cordeiro, A. B. Flores, E. W. Knightly, E. Perahia, and J. C. Widmer, "IEEE 802.11ad: Directional 60 GHz communication for multi-gigabit-per-second Wi-Fi," *IEEE Commun. Mag.*, vol. 52, no. 12, pp. 132–141, Dec. 2014.

[38] S. Sesia, I. Toufik, and M. Baker, *LTE—The UMTS Long Term Evolution: From Theory to Practice*. Hoboken, NJ, USA: Wiley, 2009.

[39] X. Yan, Y. A. Şekercioğlu, and S. Narayanan, "A survey of vertical handover decision algorithms in fourth generation heterogeneous wireless networks," *Comput. Netw.*, vol. 54, pp. 1848–1863, Feb. 2010.

[40] M. Kuhnert and C. Wietfeld, "Performance evaluation of an advanced energy-aware client-based handover solution in heterogeneous LTE and WiFi networks," in *Proc. IEEE 79th Veh. Technol. Conf. (VTC Spring)*, May 2014, pp. 1–5.

[41] A. Talukdar, M. Cudak, and A. Ghosh, "Handoff rates for millimeter-wave 5G systems," in *Proc. IEEE 79th Veh. Technol. Conf. (VTC Spring)*, May 2014, pp. 1–5.

[42] H. Song, X. Fang, and L. Yan, "Handover scheme for 5G C/U plane split heterogeneous network in high-speed railway," *IEEE Trans. Veh. Technol.*, vol. 63, no. 9, pp. 4633–4646, Nov. 2014.

[43] S. Sadr and R. S. Adve, "Handoff rate and coverage analysis in multi-tier heterogeneous networks," *IEEE Trans. Wireless Commun.*, vol. 14, no. 5, pp. 2626–2638, May 2015.

[44] P. Coucheney, E. Hyon, and J.-M. Kelif, "Mobile association problem in heterogenous wireless networks with mobility," in *Proc. IEEE 24th Int. Symp. Pers. Indoor Mobile Radio Commun. (PIMRC)*, Sep. 2013, pp. 3129–3133.

[45] C. N. Barati *et al.*, "Directional cell discovery in millimeter wave cellular networks," *IEEE Trans. Wireless Commun.*, vol. 14, no. 12, pp. 6664–6678, Dec. 2015.

[46] A. Capone, I. Filippini, and V. Sciancalepore, "Context information for fast cell discovery in mm-Wave 5G networks," in *Proc. 21st Eur. Wireless Conf.*, May 2015, pp. 1–6.

[47] A. Alkhateeb, Y.-H. Nam, M. S. Rahman, J. Zhang, and R. W. Heath, Jr., "Initial beam association in millimeter wave cellular systems: Analysis and design insights," *IEEE Trans. Wireless Commun.*, vol. 16, no. 5, pp. 2807–2821, May 2017.

[48] Y. Li, J. Luo, M. Castaneda, R. Stirling-Gallacher, W. Xu, and G. Caire. (2017). "On the beamformed broadcast signaling for millimeter wave cell discovery: Performance analysis and design insight." [Online]. Available: https://arxiv.org/abs/1709.08483

[49] M. Giordani, M. Mezzavilla, C. N. Barati, S. Rangan, and M. Zorzi, "Comparative analysis of initial access techniques in 5G mmWave cellular networks," in *Proc. Annu. Conf. Inf. Sci. Syst. (CISS)*, Princeton, NJ, USA, 2016, pp. 268–273.

[50] M. Giordani, M. Polese, A. Roy, D. Castor, and M. Zorzi, "Initial access frameworks for 3GPP NR at mmWave frequencies," in *Proc. 17th Annu. Medit. Ad Hoc Netw. Workshop (Med-Hoc-Net)*, Jun. 2018.

[51] *Evolved Universal Terrestrial Radio Access (E-UTRA) and Evolved Universal Terrestrial Radio Access Network (E-UTRAN); Overall Description; Stage 2*, document TS 36.300, 3GPP, 2018.

[52] N. Moraitis and P. Constantinou, "Indoor channel measurements and characterization at 60 GHz for wireless local area network applications," *IEEE Trans. Antennas Propag.*, vol. 52, no. 12, pp. 3180–3189, Dec. 2004.

[53] A. Patra, L. Simić, and P. Mähönen, "Smart mm-wave beam steering algorithm for fast link re-establishment under node mobility in 60 GHz indoor WLANs," in *Proc. MobiWac*, 2015, pp. 53–62.

[54] S. Ferrante, T. Deng, R. Pragada, and D. Cohen, "mm Wave initial cell search analysis under UE rotational motion," in *Proc. IEEE Int. Conf. Ubiquitous Wireless Broadband (ICUWB)*, Oct. 2015, pp. 1–7.

[55] T. S. Rappaport, G. R. Maccartney, M. K. Samimi, and S. Sun, "Wideband millimeter-wave propagation measurements and channel models for future wireless communication system design," *IEEE Trans. Commun.*, vol. 63, no. 9, pp. 3029–3056, Sep. 2015.

[56] M. K. Samimi and T. S. Rappaport, "3-D statistical channel model for millimeter-wave outdoor mobile broadband communications," in *Proc. IEEE Int. Conf. Commun. (ICC)*, Jun. 2015, pp. 2430–2436.

[57] S. Sun, T. S. Rappaport, R. W. Heath, Jr., A. Nix, and S. Rangan, "MIMO for millimeter-wave wireless communications: Beamforming, spatial multiplexing, or both?" *IEEE Commun. Mag.*, vol. 52, no. 12, pp. 110–121, Dec. 2014.

[58] T. Bai and R. W. Heath, Jr., "Coverage and rate analysis for millimeter-wave cellular networks," *IEEE Trans. Wireless Commun.*, vol. 14, no. 2, pp. 1100–1114, Feb. 2015.

[59] *Technical Specification Group Radio Access Network; Study on Scenarios and Requirements for Next Generation Access Technologies (Release 14)*, document TR 38.913, 3GPP, 2017.

[60] M. Rebato, F. Boccardi, M. Mezzavilla, S. Rangan, and M. Zorzi, "Hybrid spectrum sharing in mmWave cellular networks," *IEEE Trans. Cogn. Commun. Netw.*, vol. 3, no. 2, pp. 155–168, Jun. 2017.

[61] K. Chandra, R. V. Prasad, I. G. M. M. Niemegeers, and A. R. Biswas, "Adaptive beamwidth selection for contention based access periods in millimeter wave WLANs," in *Proc. IEEE 11th Consum. Commun. Netw. Conf. (CCNC)*, Jan. 2014, pp. 458–464.
[62] W. B. Abbas and M. Zorzi. (2016). "Towards an appropriate beamforming scheme for initial cell discovery in mmW 5G cellular networks." [Online]. Available: https://arxiv.org/abs/1605.00508
[63] W. B. Abbas, F. Gomez-Cuba, and M. Zorzi, "Millimeter wave receiver efficiency: A comprehensive comparison of beamforming schemes with low resolution ADCs," *IEEE Trans. Wireless Commun.*, vol. 16, no. 12, pp. 8131–8146, Dec. 2017.
[64] R. K. Jain, D.-M. W. Chiu, and W. R. Hawe, "A quantitative measure of fairness and discrimination for resource allocation in shared computer system," Eastern Res. Lab., Digit. Equip. Corp., Hudson, MA, USA, Tech. Rep. DEC-TR-301, 1984.

Marco Giordani (S'17) received the B.Sc. degree in information engineering and the M.Sc. degree in telecommunication engineering from the University of Padova, Italy, in 2013 and 2015, respectively, where he is currently pursuing the Ph.D. degree with the Department of Information Engineering. Since 2015, he has been a Post-Graduate Researcher with the Department of Information Engineering, University of Padova, under the supervision of Prof. M. Zorzi. In 2016, he was a Visiting Research Scholar at New York University, NY, USA. His research interests include design and validation of protocols for mobility and control-plane management in next-generation cellular networks (5G) and vehicular systems operating at millimeter waves. He received the Francesco Carassa Prize from the National Telecommunications and Information Theory Group.

Marco Mezzavilla (S'10–M'14) received the B.Sc. and M.Sc. degrees in telecommunications engineering from the University of Padova, Italy, in 2007 and 2010, respectively, and the Ph.D. degree in information engineering from the University of Padova in 2013, under the supervision of Prof. M. Zorzi. He held visiting research positions with NEC Network Laboratories, Heidelberg, Germany, in 2009, the Centre Tecnolgic Telecomunicacions Catalunya, Barcelona, Spain, in 2010, and Qualcomm Research, San Diego, CA, USA, in 2012. He holds a research scientist position with the NYU Tandon School of Engineering, where he leads various millimeter-wave (mm-wave)-related research projects mainly focusing on 5G PHY/MAC design. He has authored and co-authored multiple publications in conferences, journals, and some patent applications. His research interests include design and validation of communication protocols and applications to fourth-generation broadband wireless technologies, mm-wave communications for 5G networks, multimedia traffic optimization, radio resource management, spectrum sharing, convex optimization, cognitive networks, and experimental analysis. He has been serving as a reviewer for many IEEE conferences, journals, and magazines.

Sundeep Rangan (S'94–M'98–SM'13–F'16) received the B.A.Sc. degree from the University of Waterloo, Canada, and the M.Sc. and Ph.D. degrees from the University of California at Berkeley, CA, USA, all in electrical engineering. He has held post-doctoral appointments at the University of Michigan, Ann Arbor, MI, USA, and Bell Labs. In 2000, he co-founded (with four others) Flarion Technologies, a spin-off of Bell Labs, that developed Flash OFDM, a precursor to OFDM-based 4G cellular technologies, including LTE and WiMAX. In 2006, Flarion was acquired by Qualcomm Technologies, and he became a Director of Engineering at Qualcomm Technologies, where he was involved in OFDM infrastructure products. He joined the ECE Department, Polytechnic School of Engineering (now the NYU Tandon School of Engineering), in 2010. He is currently an Associate Professor and the Acting Director of NYU WIRELESS, a leading research center in 5G wireless systems. His research interests include wireless communications, signal processing, information theory, and control theory.

Michele Zorzi (F'07) received the Laurea and Ph.D. degrees in electrical engineering from the University of Padova in 1990 and 1994, respectively. From 1992 to 1993, he was on leave at the University of California at San Diego (UCSD). In 1993, he joined the faculty of the Dipartimento di Elettronica e Informazione, Politecnico di Milano, Italy. After spending three years with the Center for Wireless Communications, UCSD, in 1998, he joined the School of Engineering, University of Ferrara, Italy, where he became a Professor in 2000. Since 2003, he has been on the faculty of the Information Engineering Department, University of Padova. His present research interests include performance evaluation in mobile communications systems, WSN and Internet of Things, cognitive communications and networking, 5G mm-wave cellular systems, vehicular networks, and underwater communications and networks. He was a recipient of several awards from the IEEE Communications Society, including the Best Tutorial Paper Award in 2008, the Education Award in 2016, and the Stephen O. Rice Best Paper Award in 2018. He is currently the Editor-in-Chief of the IEEE TRANSACTIONS ON COGNITIVE COMMUNICATIONS AND NETWORKING. He was the Editor-in-Chief of the IEEE WIRELESS COMMUNICATIONS from 2003 to 2005 and the IEEE TRANSACTIONS ON COMMUNICATIONS from 2008 to 2011. He served as a Member-at-Large of the Board of Governors of the IEEE Communications Society from 2009 to 2011, and as its Director of Education from 2014 to 2015.